Int J CARS (2014) 9:59–69
DOI 10.1007/s11548-013-0910-y

ORIGINAL ARTICLE

# Hybrid method for the detection of pulmonary nodules using positron emission tomography/computed tomography: a preliminary study

**Atsushi Teramoto · Hiroshi Fujita · Katsuaki Takahashi · Osamu Yamamuro · Tsuneo Tamaki · Masami Nishio · Toshiki Kobayashi**

Received: 8 January 2013 / Accepted: 6 June 2013 / Published online: 23 June 2013


**Abstract**
*Purpose* In this study, an automated scheme for detecting pulmonary nodules using a novel hybrid PET/CT approach is proposed, which is designed to detect pulmonary nodules by combining data from both sets of images.
*Methods* Solitary nodules were detected on CT by a cylindrical filter that we developed previously, and in the PET imaging, high-uptake regions were detected automatically using thresholding based on standardized uptake values along with false-positive reduction by means of the anatomical information obtained from the CT images. Initial candidate nodules were identified by combining the results. False positives among the initial candidates were eliminated by a rule-based classifier and three support vector machines on the basis of the characteristic features obtained from CT and PET images.
*Results* We validated the proposed method using 100 cases of PET/CT images that were obtained during a cancer-screening program. The detection performance was assessed by free-response receiver operating characteristic (FROC) analysis.The sensitivity was 83.0 % with the number of false positives/case at 5.0, and it was 8 % higher than the sensitivity of independent detection systems using CT or PET images alone.
*Conclusion* Detection performance indicates that our method may be of practical use for the identification of pulmonary nodules in PET/CT images.

**Keywords** PET · CT · Computer-aided detection (CAD) · Pulmonary nodule

A. Teramoto (✉)
Faculty of Radiological Technology, School of Health Sciences, Fujita Health University, 1-98 Dengakugakubo, Kutsukake, Toyoake, Aichi 470-1192, Japan
e-mail: teramoto@fujita-hu.ac.jp

H. Fujita
Division of Regeneration and Advanced Medical Sciences, Department of Intelligent Image Information, Graduate School of Medicine, Gifu University, 1-1 Yanagido, Gifu 501-1194, Japan

K. Takahashi · O. Yamamuro · T. Tamaki
East Nagoya Imaging Diagnosis Center, 3-4-26 Jiyugaoka Chikusa-ku, Nagoya, Aichi 464-0044, Japan

M. Nishio · T. Kobayashi
Nagoya Radiological Diagnosis Center, 1-162 Hokke, Nakagawa-ku, Nagoya 454-0933, Japan

## Introduction

The incidence of lung cancer has been increasing, and it is the leading cause of death among males in the United States, Europe, and Japan [1]. Due to the low survival rates among lung cancer patients, it is necessary to detect and treat the cancer at an early stage. Conventional radiography has long been used to screen for lung cancer. However, small pulmonary nodules may remain undetected by this method because bone and mediastinum obscure the nodules [2]. Computed tomography (CT) is also used for lung cancer screening [3]. According to the results of a national lung screening trial [4], screening with low-dose CT scans cut lung cancer deaths by 20 %, and CT is regarded as a suitable diagnostic tool for early detection of lung cancer.

Recently, in some countries, positron emission tomography (PET)/CT has also been adopted as a mass-screening tool for diagnosis of cancers [5,6]. In this combined technique, PET images provide functional information while CT images render anatomical information, making it possible to detect small pulmonary nodules with high glucose metabolism. Wever et al. have recently reported clinical results on the effectiveness PET/CT imaging for lung tumor detection and

characterization [7]. PET/CT can be used to detect malignancy in cases of lung nodules, and it can detect nodules at the hilus pulmonis that are difficult to identify by CT alone.

Although PET/CT is a powerful diagnostic tool for cancer, it has a primary disadvantage: It generates about 1,000 slice images per scan. Since most cancer-screening cases are normal, radiologists must identify a small number of abnormal lesions from among a large number of images without any oversight. This can be cumbersome, and there is concern regarding deterioration of diagnostic accuracy or fluctuation of results.

Computer-aided detection (CAD) provides a computerized output as a "second opinion" to support a radiologist's diagnosis and is expected to assist radiologists who are required to evaluate a large number of images to identify lesions and come to a diagnosis. In this study, we focused on the automated detection of pulmonary nodules using PET/CT images.

Many researchers have developed CAD methods to detect nodules for CT [8–17], PET [18–20], and PET/CT [21,22]. For example, Lee et al. proposed a method for detecting lung nodules using CT images alone based on genetic algorithms and template matching [9], and Li et al. proposed three selective enhancement filters, for dots, lines, and planes, to simultaneously enhance objects of a specific shape while suppressing other objects [15]. Messay et al. developed a nodule detection method that incorporates a two-dimensional local contrast enhancement filter and more than 40 characteristic features [16]. We also have developed a fast detection method for pulmonary nodules using a cylindrical nodule enhancement filter (CNEF) [17]. During that process, we found that our method was approximately 4–36 times faster than the existing methods with the same or better detection capabilities and it was equivalent to or faster than the image acquisition speed of a CT unit. Similarly, several automated detection methods for high-uptake regions in whole-body PET images have been proposed [18–20]. Guan et al. developed an automated detection method for high-uptake regions based on a competition-diffusion segmentation algorithm and a mode-seeking region-growing algorithm [18]. Montgomery et al. developed a method for the automated analysis of tumors using wavelet transform and statistical methods [19]. Hara et al. proposed an automated scoring system for PET scans by using a database of the distribution of the means and standard deviations of standardized uptake values (SUVs) [20]. As for automated detection schemes using PET/CT images, Cui et al. and Ballangan et al. have each proposed different automated detection schemes for lung tumors in PET images in which the lung regions were obtained from CT images [21,22]. The previous methods described in the above studies detect the pulmonary nodules and masses from CT [8–17] or PET [18–22] images alone. In clinical settings, however, both PET and CT images are used complementarily. Therefore, automated detection using both modalities is also desirable for a CAD scheme.

Therefore, we have proposed an automated detection scheme for pulmonary nodules using both CT and PET images. The main goal of the method is to develop a basic approach for automatically detecting both malignant and benign nodules. In our pilot studies, the sensitivity of the combined method was favorable compared to those obtained by independent methods using CT or PET alone [23,24]. In the present study, we propose an improved detection scheme by introducing hybrid nodule detection and false positive (FP) reduction with three classifiers. We analyzed the detection performance using screening PET/CT images.

## Materials

In order to evaluate the detection ability of our scheme, 100 cases of PET/CT images were collected. The images were acquired during a cancer-screening program at the East Nagoya Imaging Diagnosis Center (Nagoya, Japan) using a Siemens True Point Biograph 40 PET/CT scanner (Siemens). PET images with a matrix size of $168 \times 168$ pixels (voxel size, $4.0 \times 4.0 \times 2.0\,\mathrm{mm}^3$) were obtained with free breathing and CT images with a matrix size of $512 \times 512$ pixels and voxel size of $0.97 \times 0.97 \times 2.0\,\mathrm{mm}^3$ were obtained during expiration breath-hold. These PET and CT images were aligned automatically by the PET/CT scanner. The dataset included 79 abnormal scans with pulmonary nodules and 21 normal scans. Abnormality was defined based on either one or both modalities. Among the 79 abnormal cases, there were 160 nodules detected by radiologist's standard interpretations for clinical cancer screenings. Figure 1 shows histograms of the diameters (a) and CT values (b) of nodules included from the CT images. The diameters of the nodules were measured manually using in-house software. The average diameter was 13.7 mm, and CT value was 21.8 Hounsfield units.

Of the total 100 cases, 50 cases were randomly selected and used as the training dataset for the optimization of parameters for nodule detection. Within this dataset, there was a total of 78 nodules. For an objective evaluation of the efficacy of our method for unseen cases, 50 additional PET/CT images with 82 nodules were evaluated. This study was approved by our institutional review board, and patient agreement was based on the assumption that all data were anonymized.

## Automated nodule detection

An overview of the method developed for nodule detection in PET/CT images is shown in Fig. 2. Using the proposed scheme, the pulmonary nodules were first detected separately from the given PET and CT images using specific features

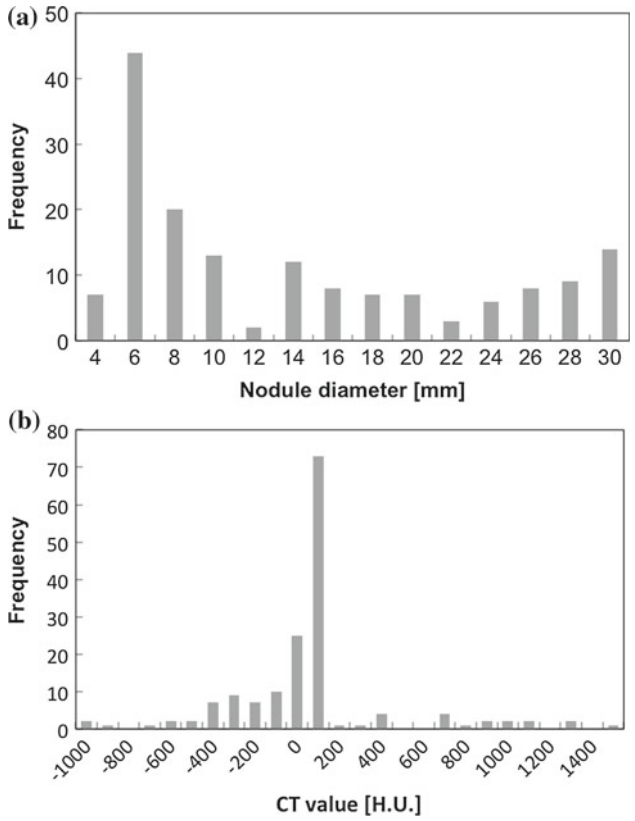


**Fig. 1** Histograms of nodule diameters (**a**) and CT values (**b**) in the dataset

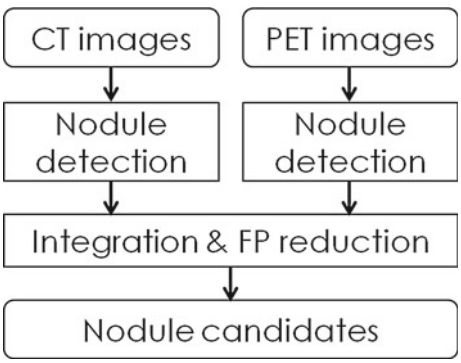


**Fig. 2** Outline of the proposed detection method

of each image. Subsequently, final candidate regions were identified by integrating the detection results of both modalities. The detection and integration methods are described as follows.

## Nodule detection in CT images

Solitary nodules, including ground glass opacity (GGO), were detected in the lung region on CT images by the main procedure shown in Fig. 3 and described elsewhere [17],

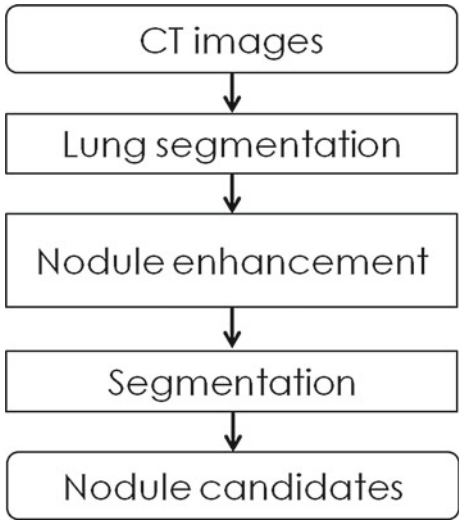


**Fig. 3** Flowchart of nodule detection in CT images

which involves the following steps: segmentation of the lung region, nodule enhancement, and nodule segmentation.

In the first step, the lung region of the CT image was automatically segmented by thresholding, and three-dimensional morphological operations and the nodules are enhanced using the unique cylindrical nodule contrast enhancement filter (CNEF) that we developed so far. The original and processed images obtained using CNEF are shown in Fig. 4. The nodule appears to have a high CT value (Fig. 4a), equivalent to those of the blood vessels. In the enhanced result (Fig. 4b), the blood vessels are suppressed, but the nodules have a selectively high CT value. The image in Fig. 4 is an example of high-contrast nodule. In addition, low-contrast nodules such as GGOs are also enhanced when there are no high-contrast objects around the nodule. After enhancement of nodule, the initial nodule regions are segmented by thresholding of enhanced images followed by labeling.

The advantage of this method is the detection speed. In the previous paper [17], detection performance and detection time of CNEF were evaluated using images from the publicly available testing database provided by the lung image database consortium (LIDC) [25]. Sensitivity was 80 % with the number of FPs/case at 4.2, and detection speed was 25–34 s per case. The detection performance of CNEF was the same or better than existing methods, and the detection time was 4–36 times faster.

## Nodule detection in PET images

The PET scanner produces images of the 3D distribution of systemic uptake of the intravenous radioactive tracer 2-deoxy-2-[18F] fluoro-D-glucose (FDG). High FDG uptake indicates that glucose metabolism is also high, and this has proven to correlate to tumor malignancy [26–28]. Thus, this

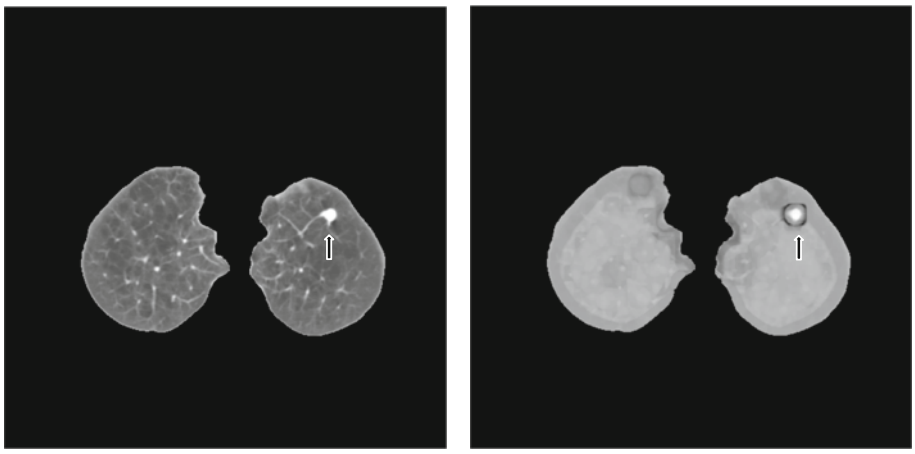

**(a)** Original image **(b)** Nodule enhanced image

**Fig. 4** Nodule enhancement with the CNEF. Original image (**a**) and nodule-enhanced image (**b**). The *arrows* indicate the detected nodules

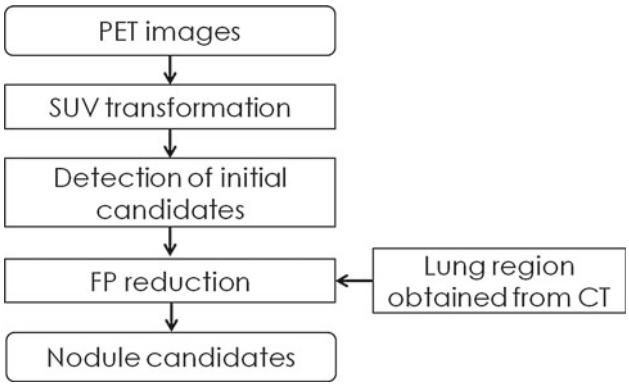


**Fig. 5** Flowchart of nodule detection in PET images

feature can be used for the characterization of tumors. However, high uptake is also observed in organs that have intrinsically high glucose metabolism (i.e., physiologic uptake), and CAD methods must account for FPs in PET images from physiologic uptake of FDG.

In the present study, high-uptake regions in the chest on PET images were detected automatically as candidate regions. Our novel detection algorithm, shown in Fig. 5, involved following steps: transformation to SUV, detection of initial candidate regions, and FP reduction.

Tissue radioactivity concentration (in kBq/mL) is available from PET images, but the measurement varies with injected dose and patient weights. Therefore, the SUV is calculated for each image as the ratio of measured activity to injected dose/patient body weight [29].

$$\mathrm{SUV} = \frac{\text{Measured activity [Bq/mL]}}{\text{Injected dose}\left[\mathrm{Bq}\right]/\text{bodyweight[g]}} \quad (1)$$

The SUV is a semi-quantitative criterion. High SUV suggests malignancy, and in the lung region, an area with a maximum SUV of $\geq$2.5 generally suspected as malignancy [30]. Here, for initial detection of candidate nodules, thresholding and labeling were performed with a threshold of SUV = 2.0 to obtain a stable region with an SUV $\geq$ 2.5. Figure 6 shows a result of initial nodule detection in PET images. Using thresholding, the nodule in the left lung was detected. However, note that initially the physiologic uptake in the myocardium, liver, and kidneys is also mistaken for high-uptake regions.

To avoid the FPs due to physiologic uptake outside the lungs, high-uptake regions inside lungs can be exclusively detected after extracting the lung regions. Although it is optimal to extract the lung regions from PET images with consideration for the transformation of the lungs due to breathing, this is very difficult to do precisely because of the poor anatomical information provided by PET scanning. In order to address this, we introduced the lung regions obtained by the CT images described in the previous section. However, the size of the lungs is also varied depending on the degree of the breathing; lung region should be determined considering this effect in order to avoid the miss detection especially around the border of lung. There is a report that the deviation of the position between PET and CT images is approximately 7.5 mm [31]. Therefore, the lung region in PET images was determined by performing the procedure where a dilation of 8 mm (2 pixels in the PET image) was applied to the original lung region detected by CT images. In 100 cases of PET/CT images, there were no missed nodules resulting from elimination by lung segmentation using the PET images.

High-uptake regions observed in the cardiac and hepatic regions outside the lungs (green color) were thus eliminated (Fig. 7), leaving the single initial candidate (red color) in the left lung, which was identified as a true finding.

### Integration and FP reduction

Initial candidate regions detected by CT and PET are represented as binary image. And then, these two images are combined by logic OR. After checking the presence of the

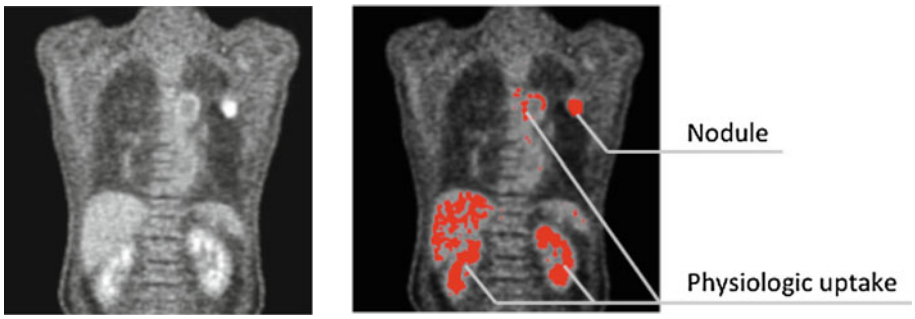


**Fig. 6** Initial nodule detection in PET images. Original image (**a**) and binarized image (**b**). Regions with SUV > 2.0 are indicated in *red*

**(a)** Original image **(b)** Binarized image

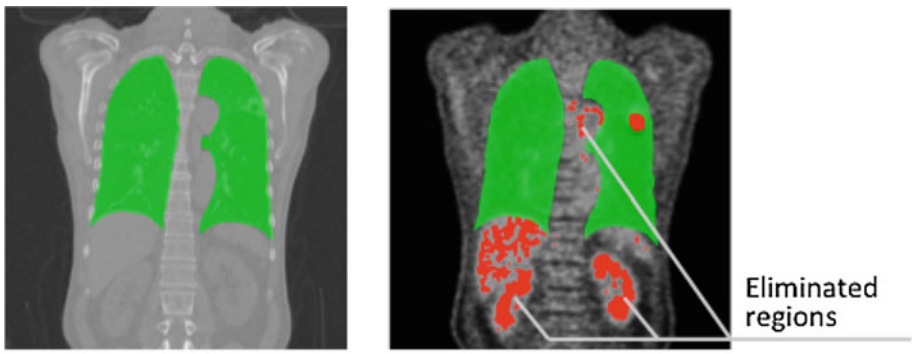


**Fig. 7** FP reduction. Lung regions were isolated by CT (**a**), and FP reduction was thus achieved (**b**)

**(a)** **(b)**

regions in both images pixel by pixel, the region detected by at least one modality is treated as a nodule. Although improvement of sensitivity by combining the two modalities was expected, the increase of FPs was a challenge at the same time. There were approximately 50 FPs per case in the initial combined candidates. Therefore, FP reduction was performed using multiple characteristic features and multistep classifiers by means of a rule-based classifier and three support vector machines (SVMs) [32].

The flow chart of this FP reduction method is shown in Fig. 8. First, characteristic values for each nodule candidate are calculated and are given to the rule-based classifier. Obvious FPs and true positives that can be easily classified using only one characteristic feature are identified. In general, the problem that should be solved by the SVM is simplified by eliminating the obvious false and true positives, which results in the improvement of classification performance.

The remaining candidates were divided into three categories: (1) nodules detected in CT images, (2) nodules detected in PET images, and (3) nodules detected by both modalities. Types of characteristic features for FP reduction depended on the above categories. For example, in case that a nodule candidate is obtained by CT images alone, the shape features from the PET images cannot be obtained because no high-uptake regions in PET images exist in the same segmented region as the one in the CT images. Therefore, we introduced the three SVMs (#1, #2, and #3) to correspond to each category. Each SVM classifies candidates into true positive (TP) and FP based on the given characteristic values. Here, the C-support vector classification (C-SVC) technique was used, and the radial basis function was used as the kernel function.

Suitable characteristic features were given for each SVM, as listed in Table 1. These features were computed based on shape and pixel values of the images. Details about these calculations in CT images are described in our previous paper [17]. Sectional area, volume, and surface area in PET images were calculated within the binarized regions using a threshold of SUV = 2.0. In Table 1, SVM #1 and SVM #2 employed characteristic features about SUV and CT values derived from undetected images, respectively. These simple features can be obtained if the center coordinates of the detected regions are known. Finally, candidate regions were obtained by merging output of the three SVMs.

## Experiments

### Evaluation methods

The detection parameters were determined using the training dataset comprising PET/CT images of 50 cases. For an objective evaluation of the efficacy of our method for unseen cases, our method was applied to additional 50 cases. As detection parameters for CT examinations, CNEF radius and the threshold for nodule detection were set at 15 mm and

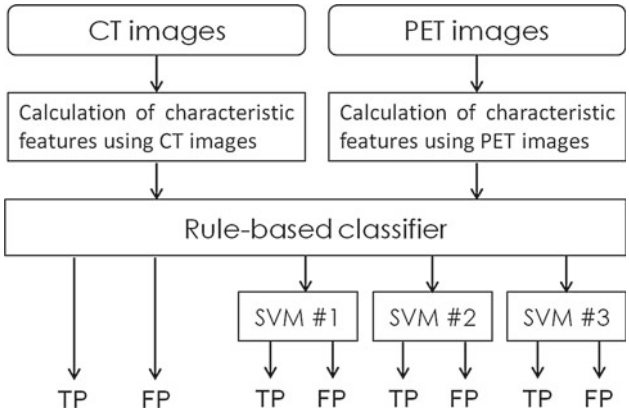


**Fig. 8** FP reduction using the rule-based classifier and 3 SVMs

**Table 1** Characteristic features for FP reduction

| Characteristic features | Selected items for SVMs | | |
|---|---|---|---|
| | SVM#1 | SVM#2 | SVM#3 |
| *Features from CT images* | | | |
| Area (X–Y, Y–Z, X–Z plane) | ✓ | | ✓ |
| Volume | ✓ | | ✓ |
| Surface area | ✓ | | ✓ |
| CT value (center) | ✓ | ✓ | ✓ |
| CT value (max) | ✓ | ✓ | ✓ |
| CT value (standard deviation) | ✓ | | ✓ |
| Convergence | ✓ | | ✓ |
| Diameter | ✓ | | ✓ |
| Overlapping area | ✓ | | ✓ |
| *Feature from PET images* | | | |
| Area (X–Y, Y–Z, X–Z plane) | | ✓ | ✓ |
| Volume | | ✓ | ✓ |
| Surface area | | ✓ | ✓ |
| SUV (center) | ✓ | ✓ | ✓ |
| SUV (max) | ✓ | ✓ | ✓ |
| SUV (mean) | | ✓ | ✓ |

75, respectively. For the PET examinations, the threshold for detection was set as SUV = 2.0. The rule-based classifier used for FP reduction was designed according to the following conditions using the training dataset:

(1) In PET detection, candidates with SUV > 10.0 were judged as TP.
(2) In CT detection, candidates whose vector concentration value was <0.4 were judged as FPs.
(3) In CT detection, candidates whose volume was <25 $mm^3$ were judged as FPs.

To the SVMs for FP reduction, we introduced the LibSVM [33] and C-SVC with the kernel of the radial basis function.

During this evaluation, the different pairs of the sensitivity and the number of FPs per case were calculated by changing the parameters (cost and gamma) for SVM, and thus, the FROC curve was obtained. Here, sensitivity was defined as the ratio of the number of detected true nodules to the number of true nodules in the database and is expressed as a percentage. Furthermore, FROC curves for CT or PET detection alone were obtained in order to compare with the combined detection. As for the FP reduction in these detections, we introduced the same method as the PET/CT detection. In FP reduction for both CT and PET detection, single images (CT or PET) can be used. Therefore, the number of characteristic values that we can obtain was restricted. We used one SVM, and the number of characteristic features was smaller than the number of features listed in Table 1. There were 9 and 6 types of features calculated in the candidate regions for CT and PET detection, respectively, and a single SVM classified the candidates into true positives and FPs using these features.

## Results

Figure 9 shows the FROC curves for CT detection, PET detection, and combined detection. Many recent CAD systems for lung nodules have been evaluated using sensitivity with FPs/case of ∼5.0. In the same way, the sensitivity for detecting nodules using only CT images in the present study was 75.0 % with FP/case = 5.0. By combining CT and PET detection, sensitivity was improved to 83.0 % with FP/case = 5.0. Therefore, the sensitivity of our hybrid scheme was 8 % greater than that of the independent detection systems using only CT images.

Figure 10 shows nodules detected in CT images. Sample 1 shows detection of a GGO that would not have shown high uptake on PET. Sample 2 indicates the detection of a

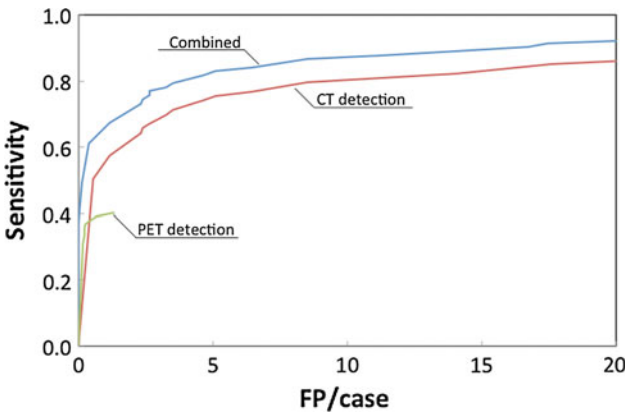


**Fig. 9** FROC curves for CT, PET, and combined detection algorithms

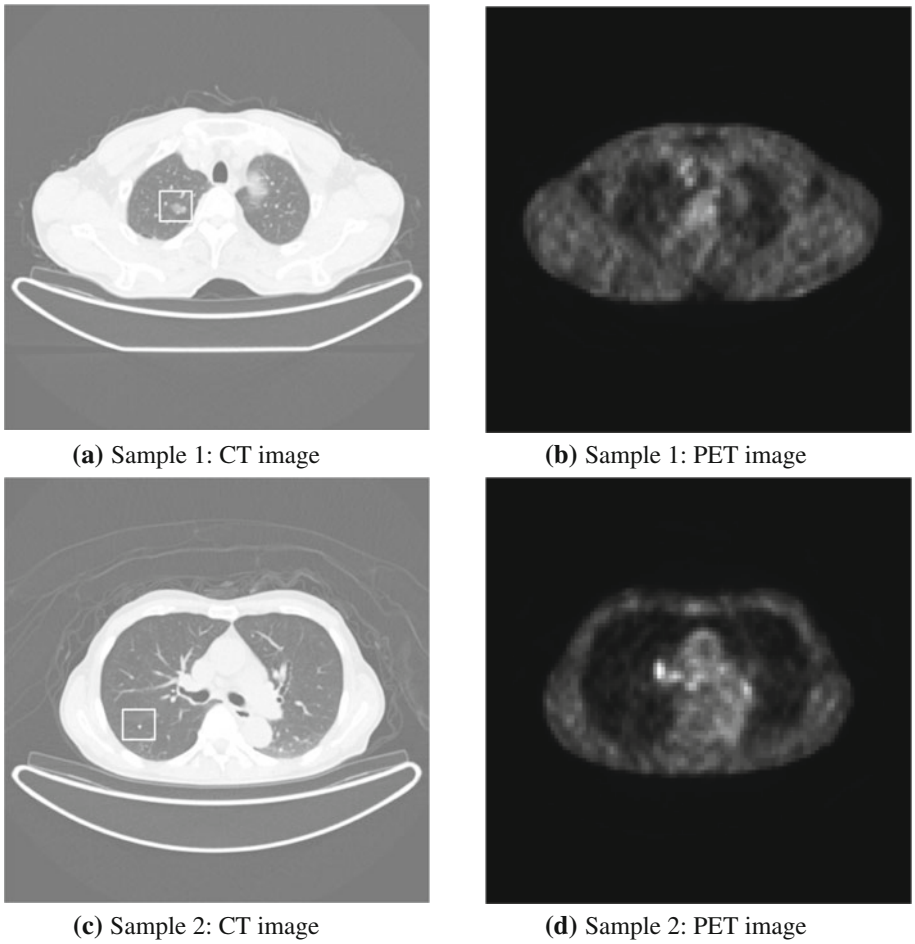

**(a)** Sample 1: CT image **(b)** Sample 1: PET image

**(c)** Sample 2: CT image **(d)** Sample 2: PET image

**Fig. 10** Nodule detected by CT images. The *boxes* indicate the nodules detected by the proposed CAD algorithm

calcified granuloma without metabolic activity. Figure 11 shows examples of nodules detected by the PET algorithms. When the nodule size increases, it becomes more likely for it to merge with blood vessels, lung wall, and mediastinum. These types of nodules become difficult to detect in CT images using the detection algorithm for solitary nodules; furthermore, significant increases in uptake can be accurately detected by PET. A nodule detected by both PET and CT images is shown in Fig. 12.

## Discussion

Because our CAD system integrates the detection abilities of 2 different types of imaging modalities, the sensitivity of our hybrid scheme is higher than that of independent detection systems using only CT or PET alone. The Venn diagram of the nodules detected by both CT and PET at a sensitivity of 83.0 % and FPs/case = 5.0 is shown in Fig. 13. As seen in the figure, 30.5 % of the nodules were detected by both CT and PET, while 46.3 and 6.1 % of the nodules were detected by CT and PET alone, respectively. These results indicate that the combination of CT and PET yields complementary results.

On the other hand, of the 82 nodules present, there were 14 that were not detected by the proposed methods. These undetected nodules are shown in Fig. 14. Most of the undetected nodules were GGOs that merged or overlapped with blood vessels or bronchi.

The nodule detection capabilities of the proposed algorithms were dependent on the nodule size and nodule contrast (visibility). In order to analyze the characteristics of the proposed method, we investigated the relationship between CT values of the nodules and sensitivity, as well as nodule diameter ($D_n$) and sensitivity.

Table 2 shows the relationship between $D_n$ and sensitivity. Here, all the nodules in the evaluation dataset were classified into two categories based on their diameter: $<10$ mm and $\geq 10$ mm. We found that most nodules with diameters $<10$ mm were detected using the CT images. PET did not detect these nodules because the SUV of small nodules decreases due to the partial volume effect. On the other hand, 76.3 % of nodules with diameters $\geq 10$ mm were detected in PET images. For the larger nodules, CT detection performance decreases because of fusing of the structures in the mediastinum and chest wall. On the other hand, PET detection performance of these larger

**(a)** Sample 3: CT image

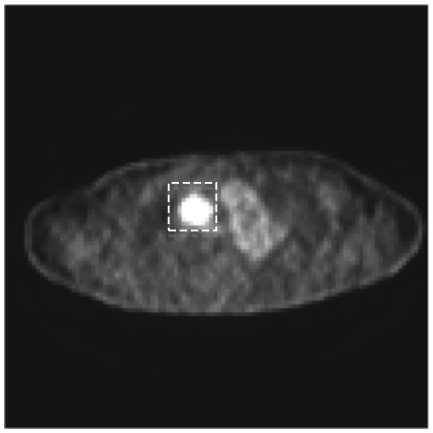

**(b)** Sample 3: PET image

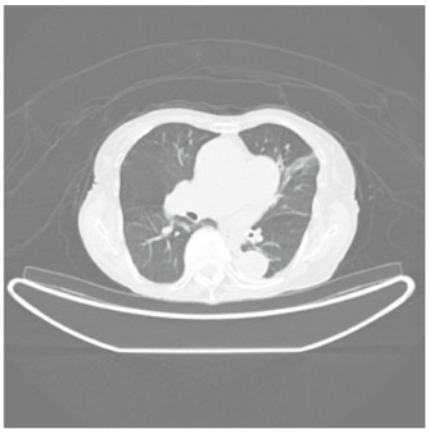

**(c)** Sample 4: CT image

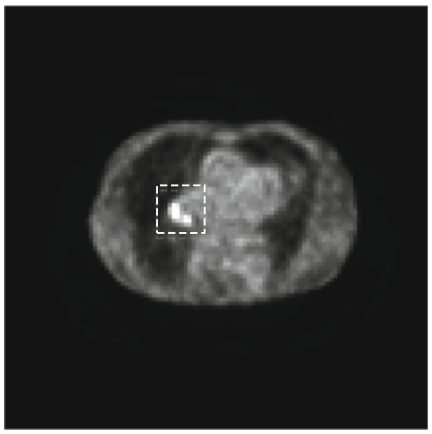

**(d)** Sample 4: PET image

**Fig. 11** Nodule detected by PET images. *Dashed boxes* indicate the nodules detected by the proposed CAD algorithm

**(a)** Sample 5: CT image

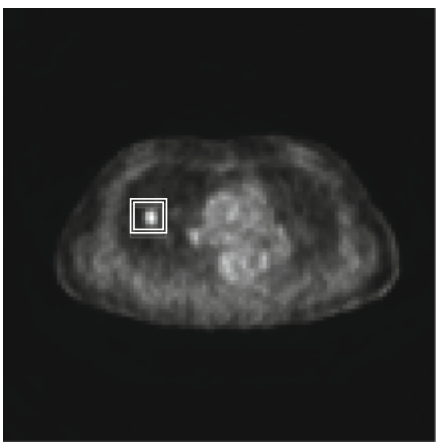

**(b)** Sample 5: PET image

**Fig. 12** Nodule detected by CT and PET images. *Double lined boxes* indicate the nodules detected by the proposed CAD method

lesions can be better because they may have high uptake values.

Next, the relationship between CT values and sensitivity was investigated. We defined $CT_{max}$ as the maximum CT value calculated inside the nodule regions identified by a radiologist. Most solid nodules have a CT value $> 0$, and GGO nodules have a CT value $< 0$ [34]. Therefore, we classified the nodules into those with $CT_{max} < 0$ and $CT_{max} \geq 0$. Table 3 shows the relationship between CT values and sensitivity. The nodules with $CT_{max} \geq 0$ were associated with slightly greater CT sensitivity compared with PET and the sensitivity of combined detection improved to 89.8 %, which indicated that the proposed method yields good results for nodules with high CT values. As for nodules with $CT_{max} < 0$,

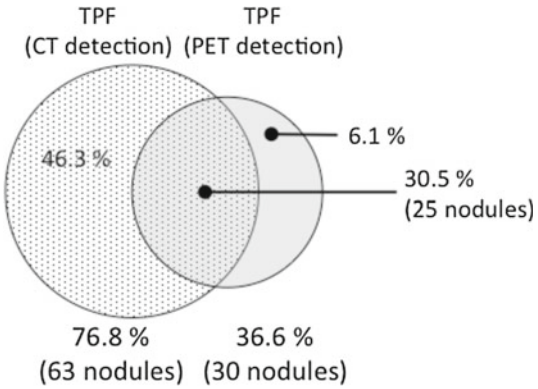


**Fig. 13** Venn diagram captures the fraction of nodules detected by our algorithms in the different modalities: 30.5 % of the nodules were detected by both CT and PET, while 46.3 and 6.1 % of the nodules were detected only by CT or PET, respectively

sensitivity of detection by PET was 18.2 %, which was much lower than the sensitivity obtained with CT. Although sensitivity of the combined result was improved to 72.7 %, the detection performance was still lower than observed for the nodules with high CT values. Detection performance for these low CT value nodules should be improved by designing and introducing alternate detection algorithms, just as lung tumors are detected and characterized by fusing PET and CT images in the practical diagnosis [7]. Nie et al. have developed semi-automated scheme for distinguishing between benign and malignant pulmonary nodules by integrating PET and CT information and have shown that diagnostic accuracy was better than CT alone or PET alone [35]. In future, we plan to develop a fused detection approach by combining clinical features related to malignancy. Consequently, we will investigate the contribution rate of all features for the nodule detection.

In order to evaluate the bias of the image dataset, we calculated the detection performance by swapping the training and evaluation datasets. As a result, the sensitivity was 83.5 % with the number of FPs/case at 4.1. This result was similar to the original result, indicating that the bias between the training and evaluation datasets was negligible.

The processing time was approximately 1 min/scan using a 2.8 GHz personal computer. This is much shorter than the data acquisition time, and the time required for the radiologist to read an image in real time. This speed could allow further detailed examinations to be performed without delay. For example, automated nodule detection could be completed

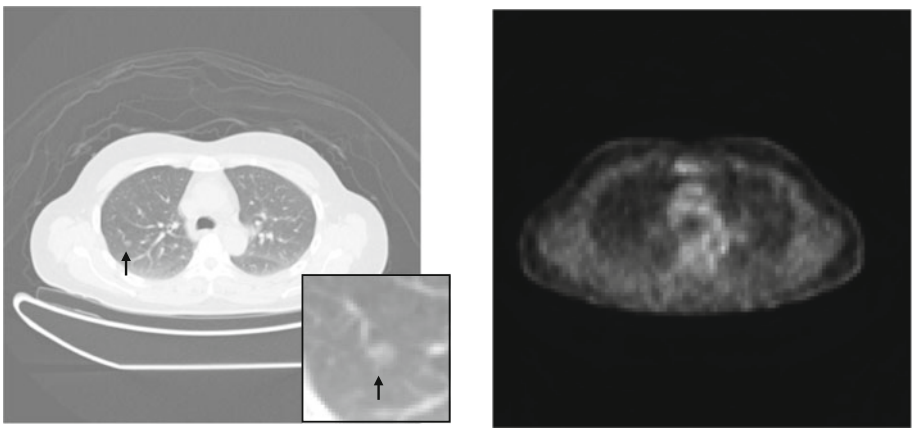

**(a)** Sample 6: CT image **(b)** Sample 6: PET image

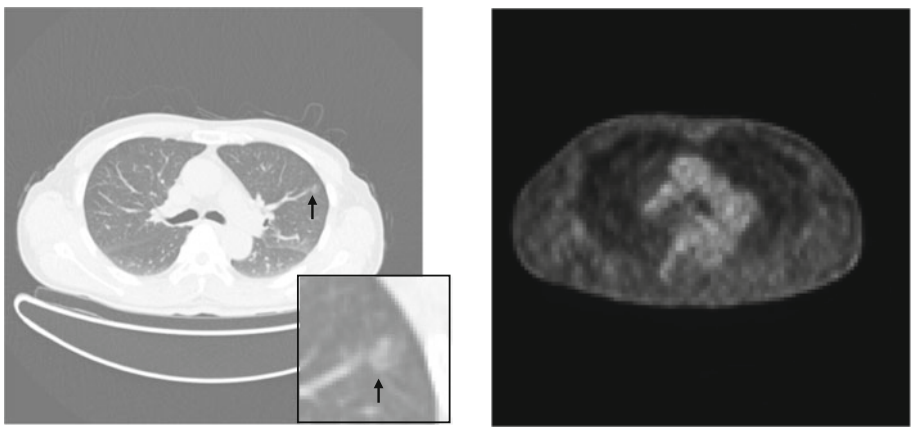

**(c)** Sample 7: CT image **(d)** Sample 7: PET image

**Fig. 14** Undetected nodules. The images show nodules that were missed by the CAD algorithms

**Table 2** Sensitivity of each detection method for nodules classified according to the nodule diameter $D_n$

| Nodule diameter $D_n$ (mm) | Sensitivity (%) | | |
|---|---|---|---|
| | CT detection | PET detection | Combined |
| $D_n < 10$ | 75.0 | 2.3 | 75.0 |
| $D_n \geq 10$ | 78.9 | 76.3 | 92.1 |

**Table 3** Sensitivity of each detection method for CT values divided into 2 ranges

| $CT_{max}$ (H.U.) | Sensitivity (%) | | |
|---|---|---|---|
| | CT detection | PET detection | Combined |
| $CT_{max} < 0$ | 69.7 | 18.2 | 72.7 |
| $CT_{max} \geq 0$ | 81.6 | 49.0 | 89.8 |

while a patient waits on the scanning bed, and if indicated by the automated result, high-resolution CT scan or a late-phase PET scan can be obtained immediately.

## Conclusions

In this study, we developed and tested a hybrid method of lung nodule detection using PET/CT images. To date, the usual scheme for pulmonary nodule detection involves imaging by either CT or PET alone. The method proposed here detects lung nodules using both the anatomical information obtained by CT and the functional information obtained with PET, as well as an interpretation procedure by radiologists. CT images detected solitary nodules using the cylindrical nodule contrast enhancement filter (CNEF) that we developed previously. The PET images were binarized based on standard uptake values (SUVs), and high-uptake regions are detected. Initial candidate nodules are identified by combining CT and PET results. False positives (FPs) among the initial candidates were eliminated using a rule-based classifier and three support vector machines (SVMs) with characteristic values obtained from CT and PET images. In the present study, we evaluated this proposed method using 100 cases of PET/CT images. We found that the sensitivity of the integrated results was 83.0 % with FPs/case = 5.0, and these results are much more desirable than those obtained via independent detection methods using CT or PET alone. In summary, the results indicate that this novel hybrid method may be useful for the detection of lung cancers, perhaps particularly in mass-screening settings.

**Acknowledgments** The authors are grateful to C.Wei-Ping and S.Tamai from Nagoya Radiological Diagnosis Center, N. Hayashi and M. Koike from Fujita Health University, and Yoya Tomita from Mie University Hospital.

**Conflict of interest** This research is supported in part by "Computational Anatomy for Computer-aided Diagnosis and Therapy: Frontiers of Medical Image Sciences" funded by Grant-in-Aid for Scientific Research on Innovative Areas, MEXT, Japan; in part by Tateishi Science and Technology Foundation, Japan.

## References

1. Ferlay J, Shin HR, Bray F, Forman D, Mathers C, Parkin DM (2008) GLOBOCAN 2008 v2.0, cancer incidence and mortality worldwide: IARC cancerBase no 10. http://globocan.iarc.fr
2. Bartjan H, Cornelia S, Hester AG, Pim AJ, Bram G et al (2010) Screening for lung cancer with digital chest radiography: sensitivity and number of secondary work-up CT examinations. Radiology 255(2):629–637
3. Sone S, Takashima S, Li F, Yang Z, Honda T et al (1998) Mass screening for lung cancer with mobile spiral computed tomography scanner. Lancet 351:1242–1245
4. National lung screening trial research team (2011) The national lung screening trial: overview and study design. Radiology 258(1):243–253
5. Ide M, Suzuki Y (2005) Is whole-body FDG-PET valuable for health screening? Eur J Nucl Med Mol Imaging 32(3):339–341
6. Lee JW, Kang KW, Paeng JC, Lee SM, Jang SJ et al (2009) Cancer screening using 18F-FDG PET/CT in Korean asymptomatic volunteers: a preliminary report. Ann Nucl Med 23(7):685–691
7. Wever W, Meylaerts L, Ceuninck L, Stroobants S, Verschakelen JA (2007) Additional value of integrated PET-CT in the detection and characterization of lung metastases: correlation with CT alone and PET alone. Eur Radiol 17:467–473
8. Niki N, Kawata Y, Kubo M (2001) A CAD system for lung cancer based on CT image. Int Congr Ser 1230:631–638
9. Con Lee Y, Hara T, Fujita H, Itoh S, Ishigaki T (2001) Automated detection of pulmonary nodules in helical CT images based on an improved template-matching technique. IEEE Trans Med Imaging 20(7):595–604
10. Suzuki K, Armato SG III, Li F, Sone S, Doi K (2003) Massive training artificial neural network (MTANN) for reduction of false positives in computerized detection of lung nodules in low-dose CT. Med Phys 30(7):1602–1617
11. Paik DS, Beaulieu CF, Rubin GD, Acar B, Jeffrey RB et al (2004) Surface normal overlap: a computer-aided detection algorithm with application to colonic polyps and lung nodules in helical CT. IEEE Trans Med Imaging 23(6):661–675
12. McNitt-Gray MF (2004) Lung nodules and beyond: approaches, challenges and opportunities in thoracic CAD. Int Congr Ser 1268:896–901
13. Con Way TW, Hadjiiski LM, Sahiner B, Chan HP, Cascade PN et al (2006) Computer-aided diagnosis of pulmonary nodules on CT scans: segmentation and classification using 3D active contours. Med Phys 33(7):2323–2337
14. Li Q (2007) Recent progress in computer-aided diagnosis of lung nodules on thin-section CT. Comput Med Imaging Graph 31(4–5):248–257
15. Li Q, Li F, Doi K (2008) Computerized detection of lung nodules in thin-section CT images by use of selective enhancement filters and an automated rule-based classifier. Acad Radiol 15(2):165–175
16. Messay T, Hardie R, Rogers S (2010) A new computationally efficient CAD system for pulmonary nodule detection in CT imagery. Med Image Anal 14(3):390–406

17. Teramoto A, Fujita H (2013) Fast lung nodule detection in chest CT images using cylindrical nodule-enhancement filter. Int J CARS 8(2):182–205
18. Guan H, Kubota T, Huang X, Zhou XS, Turk M (2006) Automatic hot spot detection and segmentation in whole body FDG-PET images. In: Proceedings of IEEE international conference on, image processing, pp 85–88
19. Montgomery DW, Amira A, Zaidi H (2007) Fully automated segmentation of oncological PET volumes using a combined multiscale and statistical model. Med Phys 34(2):722–736
20. Hara T, Kobayashi T, Kawai K, Zhou X, Ito S et al (2008) Automated scoring system of standard uptake value for torso FDG-PET. In: Proceedings of SPIE medical imaging 2008: computer-aided diagnosis, vol 6915, pp 691534-1–691534-4
21. Cui Y, Zhao B, Akhurst TJ, Yan J, Schwartz LH et al (2008) CT-guided, automated detection of lung tumors on PET images. In: Proceedings of SPIE medical imaging 2008: computer-aided diagnosis, vol 6915, pp 69152N-1–69152N-6
22. Ballangan C, Wang X, Eberl S, Fulham M, Feng D (2009) Automated detection and delineation of lung tumors in PET-CT volumes using a lung atlas and iterative mean-SUV threshold. In: Proceedings of SPIE medical imaging 2009: computer-aided diagnosis, vol 7259, pp 72593F-1–72593F-8
23. Teramoto A, Fujita H, Tomita Y, Takahashi K, Yamamuro O et al (2011) Hybrid CAD scheme for lung nodule detection in PET/CT images. In: Proceedings of SPIE medical imaging 2011: computer-aided diagnosis, vol 7963, pp 796335-1–796335-6
24. Teramoto A, Fujita H, Tomita Y, Takahashi K, Yamamuro O et al (2012) Pulmonary nodule detection in PET/CT images: improved approach using combined nodule detection and hybrid FP reduction. In: Proceedings of SPIE medical imaging 2012: computer-aided diagnosis, vol 8315, pp 83152V-1–83152V-6
25. Armato SG III, McLennan G, Bidaut L, McNitt-Gray MF, Meyer CR et al (2011) The lung image database consortium (LIDC) and image database resource initiative (IDRI): a completed reference database of lung nodules on CT scans. Med Phys 38(2):915–931
26. Kubota K, Matsuzawa T, Fujiwara T, Ito M, Hatazawa J et al (1990) Differential diagnosis of lung tumor with positron emission tomography: a prospective study. J Nucl Med 31(12):1927–1933
27. Duhaylongsod FG, Lowe VJ, Patz EF, Vaughn AL, Coleman RE et al (1995) Detection of primary and recurrent lung cancer by means of F-18 fluorodeoxyglucose positron emission tomography. J Thorac Cardiovasc Surg 110(1):130–139
28. Pauwels EK, Ribeiro MJ, Stoot JH, McCready VR, Bourguignon M et al (1998) FDG accumulation and tumor biology. Nucl Med Biol 25(4):317–322
29. Keyes JW (1995) SUV: standard uptake or silly useless value? J Nucl Med 36(10):1836–1839
30. Lowe VJ, Hoffman JM, DeLong DM, Patz EF, Coleman RE (1994) Semiquantitative and visual analysis of FDG-PET images in pulmonary abnormalities. J Nucl Med 35(11):1771–1776
31. Cohade C, Osman M, Marshall LN, Wahl RN (2003) PET-CT: accuracy of PET and CT spatial registration of lung lesions. Eur J Nucl Med Mol Imaging 30(5):721–726
32. Cristianini N, Shawe-Taylor J (2000) An introduction to support vector machines and other kernel-based learning methods. Cambridge University Press, Cambridge
33. Chang CC, Lin CJ, LIBSVM: A library for support vector machines. Software available at http://www.csie.ntu.edu.tw/~cjlin/libsvm/
34. Yamada N, Kusumoto M, Maeshima A, Suzuki K, Matsuno Y (2007) Correlation of the solid part on high-resolution computed tomography with pathological scar in small lung adenocarcinomas. Jpn J Clin Oncol 37(12):913–917
35. Nie Y, Li Q, Li F, Pu Y, Appelbaum D et al (2006) Integrating PET and CT information to improve diagnostic accuracy for lung nodules: a semiautomatic computer-aided method. J Nucl Med 47(7):1075–1080